


## REVIEW ARTICLE OPEN ACCESS

# Developments in Ultrasound-Based Imaging for Prostate Cancer Detection

Reid Vassallo<sup>1</sup>  | Miles P. Mannas<sup>2</sup> | Septimiu E. Salcudean<sup>1,2</sup> | Peter C. Black<sup>2</sup>

<sup>1</sup>School of Biomedical Engineering, University of British Columbia, Vancouver, Canada | <sup>2</sup>Department of Urologic Sciences, University of British Columbia, Vancouver, Canada

**Correspondence:** Reid Vassallo ([rvassallo@prostatecentre.com](mailto:rvassallo@prostatecentre.com))

**Received:** 23 January 2025 | **Revised:** 4 March 2025 | **Accepted:** 18 March 2025

**Funding:** This study was funded by the Natural Sciences and Engineering Research Council and the Laszlo Chair held by Professor Salcudean, UBC GF001659.

**Keywords:** elastography | micro-ultrasound | multiparametric ultrasound | photoacoustic imaging | prostate cancer

## ABSTRACT

**Background:** Prostate cancer is a significant health issue worldwide, but methods to screen for and diagnose this disease have significant inherent limitations. Some efforts to address these limitations have involved the use of ultrasound-based imaging methods.

**Methods:** This narrative review paper focuses on recent developments in the use of medical imaging, with a focus on ultrasound and related methods, to improve the diagnosis of prostate cancer. These methods include: elastography, contrast-enhanced ultrasound, targeted contrast agents, quantitative ultrasound, multiparametric ultrasound, micro-ultrasound, and photoacoustic imaging.

**Results:** This paper provides an update on clinically relevant imaging technologies which are in the technical and preclinical literature.

**Conclusion:** Novel methods and their performance are highlighted, including how they address limitations in current clinical care.

## 1 | Introduction

A diagnosis of prostate cancer (PCa) is made following a core needle biopsy performed under transrectal ultrasound (TRUS) guidance [1]. Unfortunately, TRUS reveals suspicious prostate lesions in less than half of cases because PCa often appears iso-echoic on standard B-mode ultrasound images [2, 3]. Traditional biopsy methods have therefore required regularly spaced sampling from specific zones throughout the prostate [4]. Due to this blind sampling technique, a negative result is not necessarily indicative of a lack of PCa because a cancerous lesion could be present but was not sampled by the biopsy. In fact, the false negative rate of a systematic 12-core prostate systematic template biopsy is over 30% [5], and PCa goes undetected at initial biopsy

in 18%–41% of cases [6–8]. This major gap in PCa diagnosis has led to considerable interest in new biomarkers and accessible imaging methods to better identify regions suspicious for harboring PCa that can be biopsied in a targeted fashion.

PCa is frequently visible on multiparametric magnetic resonance imaging (mpMRI), which has evolved as the current gold standard for PCa imaging [9] and has been incorporated into current biopsy regimens. In a multi-center trial patients were randomized to proceed to a standard systematic biopsy or to undergo magnetic resonance imaging (MRI) followed by targeted biopsy if a suspicious lesion was seen on MRI [10]. This study found that mpMRI-guided biopsy was superior to standard TRUS-guided biopsy. These findings have been validated

This is an open access article under the terms of the [Creative Commons Attribution-NonCommercial-NoDerivs](https://creativecommons.org/licenses/by-nc-nd/4.0/) License, which permits use and distribution in any medium, provided the original work is properly cited, the use is non-commercial and no modifications or adaptations are made.

© 2025 The Author(s). *The Prostate* published by Wiley Periodicals LLC.

in other trials [11, 12], and prebiopsy MRI has become a global standard of care where accessible.

However, there are still some limitations with using mpMRI for PCa detection. One of these is the difficult learning curve in the interpretation of mpMRI [13, 14], meaning that there is a high degree of interobserver variability in the interpretation of mpMRI and the urologists performing the biopsy procedure are often not experts at reading the MRI images [15]. Interobserver variability impacts clinical care by influencing who is referred for prostate biopsy [16]. Other limitations include the considerable cost and lack of universal access to mpMRI imaging, and inaccuracies that arise in image fusion, known as registration error. Additionally, clinically significant PCa is invisible on mpMRI in an estimated 6-15% of cases [12, 17, 18]

These remaining gaps in the standard-of-care have led researchers to look for better ways to perform targeted prostate biopsies, particularly by leveraging the lower cost and increased accessibility of ultrasound (US).

US-based modalities under investigation include elastography, contrast-enhanced ultrasound (CEUS), targeted contrast agents, quantitative ultrasound (QUS) the combination of these into multiparametric ultrasound (mpUS), micro-ultrasound (microUS) and photoacoustic imaging (PAI). Together, these advances have led to a variety of potential solutions which will be discussed in this review. Although there have been relatively recent papers reviewing US-based methods for PCa detection [19, 20], their scope has been limited to modalities which have undergone clinical assessment. This review will include emerging methods which are currently in the technical and pre-clinical literature but show promise for clinical impact in the near future.

## 2 | Addressing Unmet Needs

Although lesions suspicious for PCa are not reliably visible on B-mode TRUS, variable sources of contrast can be exploited through US, including: stiffness, increased blood flow, cell surface protein overexpression, sub-wavelength structural characteristics, and a combination thereof. These are imaged using elastography, CEUS, targeted contrast agents, QUS, and mpUS, respectively, and an overview of these methods are provided below. We also include microUS and PAI as two additional US-based methods.

### 2.1 | Elastography

Tumors are often stiffer than their surrounding healthy tissue, primarily due to an increased deposition of collagen in the extracellular matrix as a stromal response to the invading cancer [21]. This increased stiffness is the guiding principle behind manual palpation as a clinical examination technique and elastography as an imaging method for PCa detection.

Elastography is a medical imaging modality which maps the elastic properties of soft tissue from tissue deformation in

response to a mechanical excitation. Although elastography can also be performed using MRI [22–24], the use of ultrasound will be described here. The field of elastography began with strain elastography, which determined the relative strain or elasticity of tissue [25]. However, this method is only able to display relative strain and has a low sensitivity for PCa [26]. Shear wave elastography (SWE) was an improvement over this method because SWE allowed for quantitative results, and thus more sensitivity in PCa detection [27], and will be the focus here [28].

In SWE, tissue motion is introduced via a shear wave which comes from either external mechanical excitation [29], or an acoustic radiation force impulse (ARFI) generated by the imaging transducer itself [30]. Although typically performed on two-dimensional (2D) images, natively 3D methods have been developed [31], with results comparable to MRI elastography [32–34].

Meta-analyses of SWE for PCa detection have concluded a sensitivity of 83%–84%, a specificity of 85%–86%, a positive likelihood ratio of 6.02, and a negative likelihood ratio of 0.182 [19, 35]. When the SWE results are normalized with respect to the average stiffness of the prostate (to account for patient variability and differences in tissue compression), specificity was improved to 90%, with a positive predictive value of 79% and a negative predictive value of 88% [36]. However, stiffness values measured through SWE have been found to have a weak correlation with Prostate Imaging Reporting and Data System (PI-RADS) scores, which is the standard method for radiologists' interpretation of prostate mpMRI imaging [37].

### 2.2 | Bloodflow-Based Imaging

PCa is associated with an increase in microvessel density due to angiogenesis [38], and this density further increases as the cancer progresses [39–41]. There are two main ways to collect information on bloodflow using ultrasound imaging: Power Doppler US and CEUS.

Power Doppler imaging has shown an improved performance over B-mode imaging alone for PCa detection. One study found a sensitivity and specificity of 92% and 72%, respectively for Power Doppler imaging (compared to 88% and 58% for B-mode) [42]. A more recent paper used volumetric Power Doppler with a computer-aided analysis technique (VOCAL, GE Healthcare, Chicago, USA), and considered three metrics: vascularization index (VI), flow index (FI), and vascularization/flow index (VFI). At their chosen thresholds, all metrics showed promise, as VI had a sensitivity of 69% and a specificity of 90%, FI had a sensitivity of 75% and a specificity of 79%, and VFI had a sensitivity of 78% and a specificity of 83% [43].

CEUS is more often utilized in mpUS systems for PCa detection because it can better visualize the increased microvessels present in cancerous tissue [38]. In general, the second-generation contrast agents currently used in CEUS are micro-bubbles of heavy gas which are stabilized using a shell made of a lipid, protein, or a lipoprotein. These bubbles are small enough to enter the microvasculature, but large enough to prevent them from leaving the vasculature into the interstitium, so they

remain a purely intravascular contrast agent. The contrast agents used for ultrasound do not cause any hepatic or renal toxicity, as they are effectively eliminated via the lungs within 20 min of administration [44, 45].

Traditionally in CEUS, the flow of a contrast bolus into and out of the vasculature of interest is recorded one plane at a time, and the examiner then looks for signs of increased focal enhancement [46]. However, some information-containing changes in the images may be too subtle to be picked up by the unaided eye [47] so computer-aided quantification techniques have arisen to improve the interpretation of CEUS images [48, 49]. In PCa specifically, contrast ultrasound dispersion imaging (CUDI) is used because vessels resulting from cancer-induced angiogenesis tend to be small in diameter, compressible, highly tortuous, and lack a normal endothelium. These combine to cause a less efficient dispersion of blood, and therefore contrast [50]. CUDI imaging has also recently been extended to cover three dimensions [51], although it was not shown to improve diagnostic performance over standard CEUS imaging [47]. Specifically, they found a sensitivity and specificity of 81% and 64%, respectively, for CEUS, 83% and 56% for CUDI, and 83% and 55% for their combination [47].

### 2.3 | Targeted Contrast Agents

The micrometer-scale size of microbubbles keeps them confined to the blood vessel lumen, which is a desired trait for their use as a contrast agent highlighting blood flow. However, smaller structures which can escape the vasculature are being investigated to target proteins which are overexpressed on the surface of cancerous cells, such as prostate specific membrane antigen (PSMA), a common target in positron emission tomography (PET) imaging of PCa [52, 53]. This study includes promising preclinical results of PSMA-targeted nanobubbles (PSMA-NB) [54, 55], where approximately 280 nm diameter gas-filled lipid bubbles were targeted to PSMA using a small molecule ligand. They showed an increase in contrast in PSMA-expressing xenografts compared to non-PSMA expressing

tumors, while also comparing targeted and nontargeted nanobubbles.

### 2.4 | Quantitative Ultrasound

When displaying a conventional B-mode ultrasound image, only the envelope-detected signals are utilized, and only structures which are close in size to the ultrasound wavelength are displayed. However, there is much more information present in the original received echo signal, which is commonly termed the radiofrequency (RF) signal [56, 57]. This includes information regarding the structure of the tissue being imaged, which can be elucidated using QUS. Although SWE also provides quantitative information, this section refers to these images based on RF signal analysis. QUS also has the benefit of making ultrasound less user- and system-dependent [57–59] by calculating parameters which measure the attenuation and scattering of the tissue under investigation in an objective manner. Many parameters have been developed for this purpose, although not all of them have yet been applied to PCa detection. A description of the parameters which have been applied to PCa detection can be seen in Table 1, and some example images are shown in Figure 1.

There have been limited studies investigating the changes in QUS parameters caused by PCa, but Tanoue et al. found that formalin-fixed PCa specimens had lower attenuation and speed of sound than their healthy counterparts [67], while benign prostatic hyperplasia had a higher speed of sound [68]. It remains to be seen how well these findings will translate to the in vivo clinical setting. Later mpUS studies found that midband fit (a common QUS parameter whereby a line is fit to the normalized backscattered spectra [56, 69]) contributed significant information to determine areas which are suspicious for PCa [66, 70, 71].

The above-mentioned QUS examples all relied upon signal obtained in a single frame, but temporal enhanced ultrasound (TeUS) uses RF data obtained over several seconds to assess

**TABLE 1** | QUS parameters used in PCa detection.

Parameter	Description
Backscatter coefficient (BSC)	Defined as the differential scattering cross section per unit solid angle at 180 degrees per unit volume, it forms the basis of other, more specific, parameters [60]. It is also sometimes referred to as the normalized backscatter power spectrum [61].
Nakagami envelope statistics	The Nakagami model is one of several which have been proposed for statistics regarding backscattered waves (others include the Rayleigh, Rician, K, and homodyned-K distributions). One parameter in this model, called the m value, defines the shape of the distribution. As m increases, the signal moves from a pre-Rayleigh to post-Rayleigh distribution [56]. This is useful for creating maps of the Nakagami parameter [62–65].
Effective acoustic concentration (EAC) and effective scatterer diameter (ESD)	Essentially an estimation of the quantity of scattering bodies in the sample and their apparent size, obtained by fitting the BSC in the frequency domain with a scattering model [61].
Intercept, midband fit, and spectral slope	Termed Lizzi-Feleppa parameters, these come from the linear fit of the backscatter coefficient (BSC) [61].

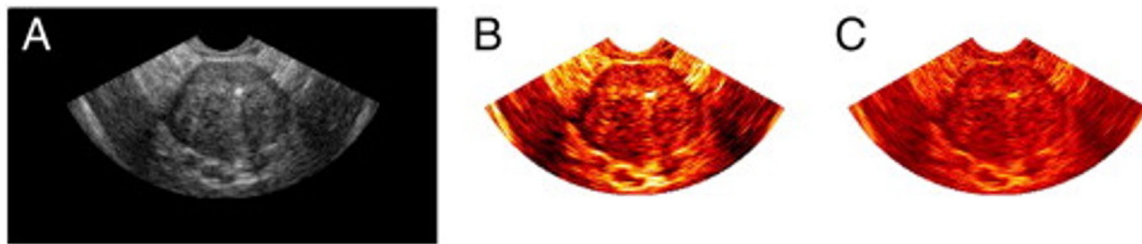


**FIGURE 1** | Various B-mode and QUS images of a prostate from the same location. (A) B-mode US image of a prostate; (B) Midband fit image of a prostate; (C) 0 MHz intercept image of the prostate. Image adapted with permission from [66]. [Color figure can be viewed at [wileyonlinelibrary.com](http://wileyonlinelibrary.com)]

**TABLE 2** | Parameters used in recent mpUS studies.

Study	Parameters used
Fulgham [76]	B-mode, Color Doppler
Mannaerts et al. [77]	B-mode, CEUS, Elastography
Morris et al. [78]	B-mode, Elastography
Pepe et al. [79]	B-mode, CEUS, Elastography
Morris et al. [70]	B-mode, Midband Fit, Elastography
Chan et al. [71]	B-mode, Midband Fit, Elastography
Wildeboer et al. [80]	B-mode, CEUS, Elastography
Liang et al. [81]	B-mode, Elastography
Chan et al. [82]	B-mode, Midband Fit, Elastography
Jung et al. [83]	B-mode, Color Doppler, Power Doppler
Chen et al. [84]	CEUS, Elastography
Chan et al. [85]	B-mode, Midband Fit, Elastography

tissue characteristics using an underlying machine learning (ML) framework [72]. The TeUS signature of a tissue is dependent on its scattering function and the inverse of its shear modulus elasticity [73, 74]. Previous studies have shown that TeUS and single-frame RF analysis are complementary [72, 75], although TeUS showed better performance [73]. The best results in PCa detection using TeUS so far were published in 2018 using a recurrent neural network (RNN) to explicitly analyze TeUS data in the temporal domain, resulting in a sensitivity of 76%, specificity of 98%, and accuracy of 93% on 255 prostate biopsy cores from 157 patients [73].

## 2.5 | Multiparametric Ultrasound

As the field of mpUS imaging of PCa is still very much in development, there has been no consensus regarding which parameters should be included. This makes it difficult to compare results between papers, as each will include different types of information in their imaging, which can be seen in Table 2. Also, the metrics used to present the results tend to differ between the clinical and engineering literature. Nonetheless, there are a few key trends that can be noted.

First, it is commonly found that the combination of various types of information in mpUS outperforms any single parameter on its own [71, 77, 82, 85], which bodes well for mpUS development. However, it has not yet been shown to be equivalent to mpMRI [86, 87], as demonstrated by the most recent randomized controlled trial (RCT) that reported the detection of 4.3% fewer cases of csPCa with mpUS than mpMRI [88].

Second, there appear to be two main ways that the various types of information are presented to the viewer. One way is similar to other types of multiparametric imaging currently in clinical practice such as mpMRI, where they are analyzed as separate images and the clinician combines their findings from each of the parameters, either mentally or using a formal scoring system [76, 77, 79, 81, 83, 86, 88]. This was utilized in two of the seminal RCTs on this subject, the Imperial Prostate 1 Prostate Cancer Screening Trial Using Imaging (IP1-PROSTAGRAM) and Cancer Diagnosis by Multiparametric Ultrasound of the prostate (CADMUS) [86, 88].

The other way is to combine the information gleaned from each parameter into one image to display to the clinician [70, 71, 78, 82, 84], or use these combined features in a ML classification algorithm [80]. Studies by Chan et al. and Morris et al. used a linear combination of parameters to create a unified image, with the weighting for this combination found using ML [70] or an unconstrained minimization routine on a training subset [71]. This then progressed to using a deep neural network to directly combine the various parameters into a single image [82].

These methods for combining parameters into a single image still reside in the technical literature and have not yet made their way into the clinical literature. However, an image which combines information sources into one image (indirectly) depicting how suspicious each pixel is of PCa would be very useful for applications such as real-time targeted biopsy guidance. This concept is not completely novel to PCa imaging either, as it is very similar to the cancer probability map based on mpMRI findings which was introduced by Moradi et al. [89].

## 2.6 | Micro-Ultrasound

MicroUS uses a 29 MHz side-fire probe to image the prostate, as opposed to the usual 9–12 MHz frequency used in urologic ultrasound [90]. This increased frequency allows for imaging of the peripheral zone of the prostate at a resolution of 70  $\mu\text{m}$ ,



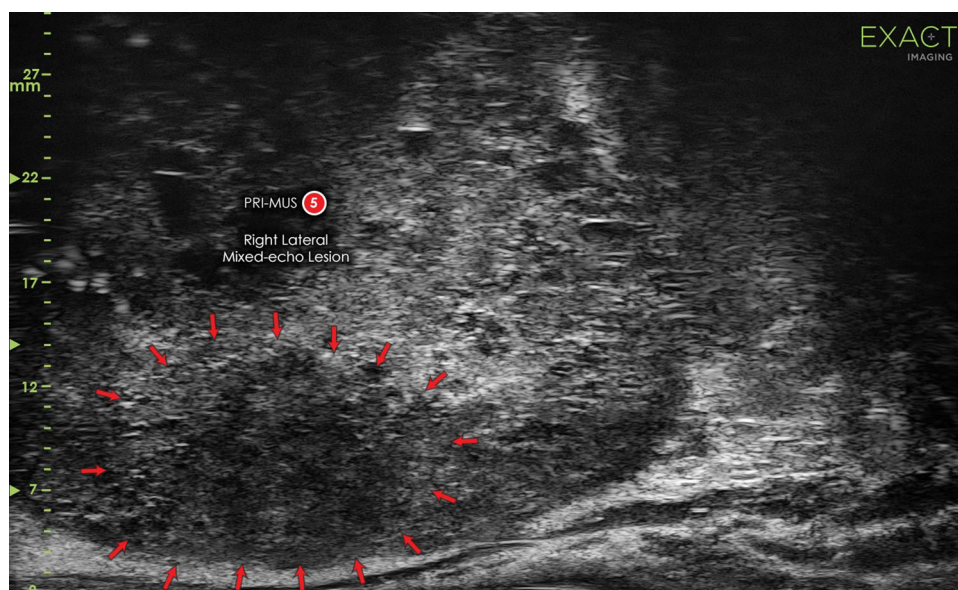


**FIGURE 2** | An example microUS image, with red arrows indicating the primary lesion. [Color figure can be viewed at [wileyonlinelibrary.com](http://wileyonlinelibrary.com)]

which is approximately the size of the ducts in the prostate [19]. This means that microUS can identify subtle variations in the ductal structure caused by cancer which are not visible on traditional ultrasound systems. An example of a microUS image can be seen in Figure 2. A grading system for prostate lesions on microUS, called Prostate Risk Identification using Micro-ultrasound (PRI-MUS) has been developed, and it is analogous to the PI-RADS score used to interpret mpMRI [91]. A considerable number of non-randomized studies have been performed comparing microUS to mpMRI for targeted prostate biopsy, including a multicenter prospective analysis of 1040 patients [91] and two meta-analyses [92, 93]. These all concluded that microUS demonstrated equivalent performance to mpMRI for prostate biopsy targeting. Another recent study compared microUS to retrospectively and prospectively read mpMRI, using whole mount histopathology as the ground truth. They found that microUS outperformed both mpMRI reading methods for index lesion identification [94]. An ongoing RCT called Optimization of prostate biopsy - Micro-Ultrasound versus MRI (OPTIMUM) [95] is the first prospective and randomized trial in this domain. This study will compare microUS-guided biopsy with MRI/US fusion biopsy and MRI/microUS “contour-less” fusion biopsy, which is an image fusion biopsy method where the prostate does not need to be segmented in the MRI image before the procedure. Since several high quality RCTs have demonstrated the clinical utility of mpMRI in the diagnostic pathway of PCa, it will be critical to have high quality RCT results to justify using microUS in the place of mpMRI.

Rohrbach et al. implemented many of the QUS parameters listed in Table 1 on a microUS scanner and found that the most useful parameters of the ones they assessed were envelope statistics using a Nakagami distribution, effective scatterer diameter (ESD), and effective acoustic concentration (EAC) [96]. However, we cannot reliably differentiate whether the diagnostic performance primarily came from QUS or the superior spatial resolution of microUS. There have also been proof-of-concept efforts to implement elastography using

microUS, but these do not yet have data regarding their clinical effectiveness [97, 98].

One trade-off that is inherent to ultrasound imaging is that of depth versus resolution. Imaging with a higher frequency (such as in microUS) provides better resolution but cannot penetrate as far into tissue which limits the usable depth of the image to 6 cm. The opposite is true for imaging at lower frequencies (better penetration depth but worse image resolution). This has led to microUS initially only being indicated to image the peripheral zone of the prostate. However, a PRI-MUS scoring system for the anterior prostate has since been introduced and undergone initial validation [99], adding to the previous anecdotal evidence suggesting the anterior and transition zones are adequately visible with microUS [100].

## 2.7 | Photoacoustic Imaging

Another acoustic imaging modality closely related to conventional ultrasound is PAI, where a repeating near-infrared (NIR) pulse is directed at the imaging target, which causes it to undergo elastic expansion from local heating. This sends pressure waves through the medium which can be detected with ultrasonic transducers and then reconstructed into images. The optical irradiation of this system allows for better contrast among different types of biological tissue than typical ultrasound imaging, while receiving ultrasonic signals overcomes the short penetration depth and large degree of scattering which are the typical shortfalls of purely optical-based imaging [101].

Based on the optical scattering properties of the prostate, the accepted penetration depth of prostate PAI is 3–5 cm [102], and since the prostate sits deeper to the surface of the skin than this [103] an internal illumination strategy is required. Although a transrectal light delivery and ultrasound detection strategy is the most convenient and least invasive, transurethral illumination with transrectal ultrasound detection leads to better results because it reduces the total distance that the energy must travel [101].

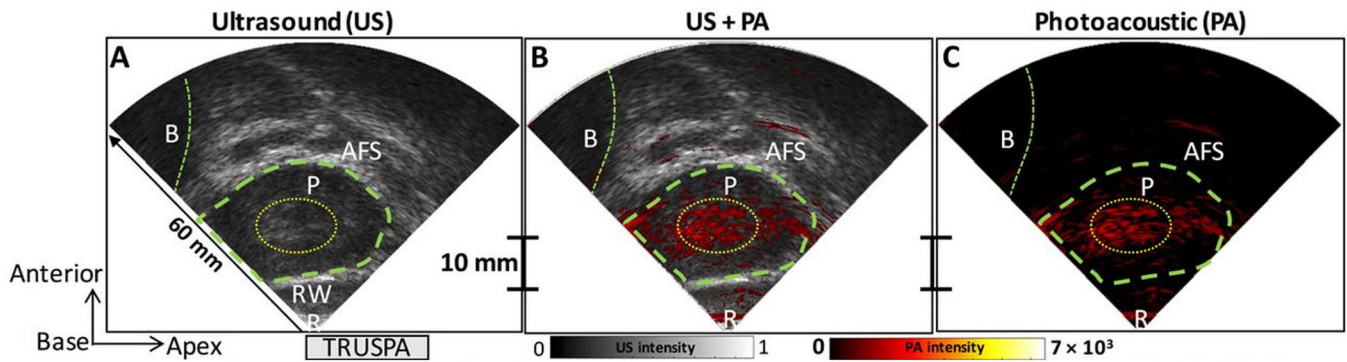


**FIGURE 3** | Example images from a PA system. The B-mode US image is seen in greyscale in (A), the PA image is shown in red color scale in (C), and overlaid onto the B-mode image in (B). Labeled anatomical structures of interest are: bladder (B), prostate (P), rectum (R), rectal wall (RW), and the anterior fibromuscular stroma (AFS). Image adapted with permission from [112]. [Color figure can be viewed at [wileyonlinelibrary.com](https://onlinelibrary.wiley.com)]

PCa can be imaged using either endogenous or exogenous contrast. Due to its good optical absorption, hemoglobin in red blood cells is often used to identify cancer using PAI [104], because of the angiogenesis present in cancerous tissue that has been discussed previously. Dogra et al. imaged ex-vivo prostate specimens using multi-spectral PAI (the wavelengths used were 760 nm, 850 nm, 930 nm and 970 nm), and differentiated malignant and nonmalignant tissue with a sensitivity of 81.3% and specificity of 96.2% [105]. Exogenous contrast agents such as NIR dyes or gold nanoparticles, however, can enhance the PAI signal and increase its utility in PCa [106–109].

Some PAI contrast agents specifically target receptors which are commonly overexpressed in human PCa cells. Specifically, these are gastrin-releasing peptide receptor (GRPR) [110], and PSMA [111]. GRPR is targeted using AA3G-740, which was developed by Levi et al., and is based on a fluorescent dye (ATTO-740) linked to the gastrin-releasing peptide (GRP) [101]. The use of AA3G-740 caused a nearly twofold increase in PAI signals in mice in vivo [106]. PSMA, meanwhile, can be leveraged by attaching the IRDye800CW to agents which specifically target PSMA [101].

Hardware developments in PAI include the development of a transrectal probe which can be used for both transrectally-illuminated PAI and ultrasound imaging [112], images from which can be seen in Figure 3. The probe was used in a study that also employed indocyanine green (ICG) as a PAI contrast agent, which is commonly used for fluorescence imaging in applications such as neurovascular surgery [113] and ophthalmology [114].

### 3 | Conclusions

The global burden of PCa is significant, but considerable deficits remain in our ability to screen for and diagnose this disease. Imaging has shown a great deal of promise in addressing the shortcomings of earlier screening and diagnosis methods by visualizing the prostate and allowing for more effective targeting of suspicious lesions. Although good results are shown by mpMRI, this modality is associated with a difficult learning curve, high interobserver variability, reliance on potentially inaccurate fusion technologies, high cost and poor access in

many communities, leading to many efforts to develop enhanced ultrasound techniques to detect PCa. The development of novel ultrasound-based imaging modalities such as elastography, CEUS, PSMA-NB, and QUS have added information which increase the clinician's ability to identify cancerous regions, and their combination in mpUS outperforms any single modality alone. MicroUS has shown performance equivalent to mpMRI for prostate biopsy targeting, which makes it a very promising technology which should be further explored. Newer developments in PAI are also very compelling and it remains an active area of research. Overall, these ultrasound-based methods show favorable results to detect PCa with performance approaching that of mpMRI but in a more accessible manner.

### Acknowledgments

Thank you to Dr. Brian Wodlinger for providing the microUS image. This study was funded by the Natural Sciences and Engineering Research Council and the Laszlo Chair held by Professor Salcudean, UBC GF001659.

### Conflicts of Interest

The authors declare no conflicts of interest.

### Data Availability Statement

The authors have nothing to report.

### References

1. J. I. Izawa, L. Klotz, D. R. Siemens, et al., "Prostate Cancer Screening: Canadian Guidelines 2011," *Canadian Urological Association Journal* 5, no. 4 (2011): 235–240, <https://doi.org/10.5489/cuaj.11134>.
2. R. Onur, P. J. Littrup, J. E. Pontes, and F. J. Bianco, "Contemporary Impact of Transrectal Ultrasound Lesions for Prostate Cancer Detection," *Journal of Urology* 172, no. 2 (2004): 512–514, <https://doi.org/10.1097/01.ju.00000131621.61732.6b>.
3. M. Otori, M. W. Kattan, T. Utsunomiya, K. Suyama, P. T. Scardino, and T. M. Wheeler, "Do Impalpable Stage T1c Prostate Cancers Visible on Ultrasound Differ From Those Not Visible?," *Journal of Urology* 169, no. 3 (2003): 964–968, <https://doi.org/10.1097/01.ju.0000049963.28489.ab>.
4. N. Mottet, R. C. N. van den Bergh, E. Briers, et al., "EAU-EANM-ESTRO-ESUR-SIOG Guidelines on Prostate Cancer—2020 Update. Part 1: Screening, Diagnosis, and Local Treatment With Curative Intent,"

- European Urology 79, no. 2 (2021): 243–262, <https://doi.org/10.1016/j.eururo.2020.09.042>.
5. E. C. Serefoglu, S. Altinova, N. S. Ugras, E. Akincioglu, E. Asil, and D. Balbay, “How Reliable Is 12-core Prostate Biopsy Procedure in the Detection of Prostate Cancer?,” *Canadian Urological Association Journal* 7, no. 5–6 (2013): 293, <https://doi.org/10.5489/cuaj.11224>.
6. J. L. Campos-Fernandes, L. Bastien, N. Nicolaiew, et al., “Prostate Cancer Detection Rate in Patients With Repeated Extended 21-Sample Needle Biopsy,” *European Urology* 55, no. 3 (2009): 600–609, <https://doi.org/10.1016/j.eururo.2008.06.043>.
7. F. H. Schröder, H. B. Carter, T. Wolters, et al., “Early Detection of Prostate Cancer in 2007,” *European Urology* 53, no. 3 (2008): 468–477, <https://doi.org/10.1016/j.eururo.2007.10.047>.
8. J. Walz, M. Graefen, F. K. Chun, et al., “High Incidence of Prostate Cancer Detected by Saturation Biopsy After Previous Negative Biopsy Series,” *European Urology* 50, no. 3 (2006): 498–505, <https://doi.org/10.1016/j.eururo.2006.03.026>.
9. G. Giannarini, A. Crestani, M. Rossanese, and V. Ficarra, “Multiparametric Magnetic Resonance Imaging Targeted Biopsy for Early Detection of Prostate Cancer: All That Glitters Is Not Gold,” *European Urology* 71, no. 6 (2017): 904–906, <https://doi.org/10.1016/j.eururo.2017.01.010>.
10. V. Kasivisvanathan, A. S. Rannikko, M. Borghi, et al., “MRI-Targeted or Standard Biopsy for Prostate-Cancer Diagnosis,” *New England Journal of Medicine* 378, no. 19 (2018): 1767–1777, <https://doi.org/10.1056/NEJMoa1801993>.
11. L. Klotz, J. Chin, P. C. Black, et al., “Comparison of Multiparametric Magnetic Resonance Imaging–Targeted Biopsy With Systematic Transrectal Ultrasonography Biopsy for Biopsy-Naïve Men at Risk for Prostate Cancer: A Phase 3 Randomized Clinical Trial,” *JAMA Oncology* 7, no. 4 (2021): 534–542, <https://doi.org/10.1001/jamaoncol.2020.7589>.
12. L. Klotz, J. Chin, P. C. Black, et al., “Magnetic Resonance Imaging–Targeted Versus Systematic Prostate Biopsies: 2-Year Follow-Up of a Prospective Randomized Trial (PRECISE),” *European Urology Oncology* 7, no. 3 (2023): 456–461, <https://doi.org/10.1016/j.euo.2023.09.013>.
13. G. Gaziev, K. Wadhwa, T. Barrett, et al., “Defining the Learning Curve for Multiparametric Magnetic Resonance Imaging (MRI) of the Prostate Using Mri-Transrectal Ultrasonography (TRUS) Fusion-Guided Transperineal Prostate Biopsies as a Validation Tool,” *BJU International* 117, no. 1 (2016): 80–86, <https://doi.org/10.1111/bju.12892>.
14. A. B. Rosenkrantz, A. Ayoola, D. Hoffman, et al., “The Learning Curve in Prostate MRI Interpretation: Self-Directed Learning Versus Continual Reader Feedback,” *American Journal of Roentgenology* 208, no. 3 (2017): W92–W100, <https://doi.org/10.2214/AJR.16.16876>.
15. A. Annamalai, J. N. Fustok, J. Beltran-Perez, A. T. Rashad, L. S. Krane, and B. L. Triche, “Interobserver Agreement and Accuracy In Interpreting mpMRI of the Prostate: A Systematic Review,” *Current Urology Reports* 23, no. 1 (2022): 1–10, <https://doi.org/10.1007/s11934-022-01084-y>.
16. B. Rosenzweig, Y. Laitman, D. E. Zilberman, et al., “Effects of “Real Life” Prostate MRI Inter-Observer Variability on Total Needle Samples and Indication for Biopsy,” *Urologic Oncology* 38, no. 10 (2020): 793, <https://doi.org/10.1016/j.urolonc.2020.03.015>.
17. M. A. Liss, L. F. Newcomb, Y. Zheng, et al., “Magnetic Resonance Imaging for the Detection of High Grade Cancer in the Canary Prostate Active Surveillance Study,” *Journal of Urology* 204, no. 4 (2020): 701–706, <https://doi.org/10.1097/JU.0000000000001088>.
18. C. Dariane, G. Ploussard, E. Barret, et al., “Micro-Ultrasound-Guided Biopsies Versus Systematic Biopsies in the Detection of Prostate Cancer: A Systematic Review and Meta-Analysis,” *World Journal of Urology* 41, no. 3 (2023): 641–651, <https://doi.org/10.1007/s00345-022-04087-z>.
19. A. B. Dias, C. O'Brien, J. M. Correias, and S. Ghai, “Multiparametric Ultrasound and Micro-Ultrasound In Prostate Cancer: A Comprehensive Review,” *British Journal of Radiology* 95, no. 1131 (2021): 20210633, <https://doi.org/10.1259/bjr.20210633>.
20. M. Kaneko, M. S. L. Lenon, L. Storino Ramacciotti, et al., “Multiparametric Ultrasound of Prostate: Role in Prostate Cancer Diagnosis,” *Therapeutic Advances in Urology* 14 (2022): 17562872221145625, <https://doi.org/10.1177/17562872221145625>.
21. J. A. Tuxhorn, G. E. Ayala, M. J. Smith, V. C. Smith, T. D. Dang, and D. R. Rowley, “Reactive Stroma in Human Prostate Cancer: Induction of Myofibroblast Phenotype and Extracellular Matrix Remodeling,” *Clinical Cancer Research: An Official Journal of the American Association for Cancer Research* 8, no. 9 (2002): 2912–2923.
22. R. S. Sahebjavaher, A. Baghani, M. Honarvar, R. Sinkus, and S. E. Salcudean, “Transperineal Prostate MR Elastography: Initial In Vivo Results,” *Magnetic Resonance in Medicine* 69, no. 2 (2013): 411–420, <https://doi.org/10.1002/mrm.24268>.
23. R. S. Sahebjavaher, S. Frew, A. Bylinskii, et al., “Prostate MR Elastography With Transperineal Electromagnetic Actuation and a Fast Fractionally Encoded Steady-State Gradient Echo Sequence,” *NMR in Biomedicine* 27, no. 7 (2014): 784–794, <https://doi.org/10.1002/nbm.3118>.
24. R. Reiter, S. Majumdar, S. Kearney, et al., “Investigating the Heterogeneity of Viscoelastic Properties in Prostate Cancer Using MR Elastography at 9.4T in Fresh Prostatectomy Specimens,” *Magnetic Resonance Imaging* 87 (2022): 113–118, <https://doi.org/10.1016/j.mri.2022.01.005>.
25. R. G. Barr, “Sonographic Breast Elastography,” *Journal of Ultrasound in Medicine: Official Journal of the American Institute of Ultrasound in Medicine* 31, no. 5 (2012): 773–783, <https://doi.org/10.7863/jum.2012.31.5.773>.
26. J. Schiffmann, M. Grindei, Z. Tian, et al., “Limitations of Elastography Based Prostate Biopsy,” *Journal of Urology* 195, no. 6 (2016): 1731–1736, <https://doi.org/10.1016/j.juro.2015.12.086>.
27. D. J. Tyloch, J. F. Tyloch, J. Adamowicz, et al., “Comparison of Strain and Shear Wave Elastography in Prostate Cancer Detection,” *Ultrasound in Medicine & Biology* 49, no. 3 (2023): 889–900, <https://doi.org/10.1016/j.ultrasmedbio.2022.11.015>.
28. M. Moradi, S. S. Mahdavi, G. Nir, et al., “Multiparametric 3D In Vivo Ultrasound Vibroelastography Imaging of Prostate Cancer: Preliminary Results,” *Medical Physics* 41, no. 7 (2014): 073505, <https://doi.org/10.1118/1.4884226>.
29. H. Zhao, P. Song, D. D. Meixner, et al., “External Vibration Multi-Directional Ultrasound Shearwave Elastography (EVMUSE): Application in Liver Fibrosis Staging,” *IEEE Transactions on Medical Imaging* 33, no. 11 (2014): 2140–2148, <https://doi.org/10.1109/TMI.2014.2332542>.
30. M. Lupsor, R. Badea, H. Stefanescu, et al. Performance of a New Elastographic Method (ARFI technology) Compared to Unidimensional Transient Elastography in the Noninvasive Assessment of Chronic Hepatitis C. Preliminary Results.
31. A. Baghani, H. Eskandari, W. Wang, et al., “Real-Time Quantitative Elasticity Imaging of Deep Tissue Using Free-Hand Conventional Ultrasound,” in *Medical Image Computing and Computer-Assisted Intervention – MICCAI 2012*, eds. N. Ayache, H. Delingette, P. Golland, K. Mori. Springer, 2012, 617–624, [https://doi.org/10.1007/978-3-642-33418-4\\_76](https://doi.org/10.1007/978-3-642-33418-4_76).
32. Q. Zeng, M. Honarvar, C. Schneider, et al., “Three-Dimensional Multi-Frequency Shear Wave Absolute Vibro-Elastography (3D S-WAVE) With a Matrix Array Transducer: Implementation and Preliminary In Vivo Study of the Liver,” *IEEE Transactions on Medical Imaging* 40, no. 2 (2021): 648–660, <https://doi.org/10.1109/TMI.2020.3034065>.



33. T. A. Aleef, J. Lobo, A. Baghani, et al., "Multi-Frequency 3D Shear Wave Absolute Vibro-Elastography (S-WAVE) System for the Prostate," *IEEE Transactions on Medical Imaging* 34, no. 11 (2023): 3436–3450, <https://doi.org/10.1109/TMI.2023.3288468>.
34. T. A. Aleef, Q. Zeng, H. Moradi, et al., "3D Transducer Mounted Shear Wave Absolute Vibro-Elastography: Proof of Concept," *IEEE Transactions on Ultrasonics, Ferroelectrics, and Frequency Control* 70, no. 9 (2023): 1026–1038, <https://doi.org/10.1109/TUFFC.2023.3249795>.
35. S. Woo, C. H. Suh, S. Y. Kim, J. Y. Cho, and S. H. Kim, "Shear-Wave Elastography for Detection of Prostate Cancer: A Systematic Review and Diagnostic Meta-Analysis," *American Journal of Roentgenology* 209, no. 4 (2017): 806–814, <https://doi.org/10.2214/AJR.17.18056>.
36. D. C. Morris, D. Y. Chan, M. L. Palmeri, T. J. Polascik, W. C. Foo, and K. R. Nightingale, "Prostate Cancer Detection Using 3-D Shear Wave Elasticity Imaging," *Ultrasound in Medicine and Biology (Oxford)* 47, no. 7 (2021): 1670–1680, <https://doi.org/10.1016/j.ultrasmedbio.2021.02.006>.
37. W. Ageeli, C. Wei, X. Zhang, et al., "Quantitative Ultrasound Shear Wave Elastography (USWE)-Measured Tissue Stiffness Correlates With PIRADS Scoring of MRI and Gleason Score on Whole-Mount Histopathology of Prostate Cancer: Implications for Ultrasound Image-Guided Targeting Approach," *Insights into Imaging* 12, no. 1 (2021): 96, <https://doi.org/10.1186/s13244-021-01039-w>.
38. L. Pallwein, M. Mitterberger, A. Pelzer, et al., "Ultrasound of Prostate Cancer: Recent Advances," *European Radiology* 18, no. 4 (2008): 707–715, <https://doi.org/10.1007/s00330-007-0779-7>.
39. N. Weidner, P. R. Carroll, J. Flax, W. Blumenfeld, and J. Folkman, "Tumor Angiogenesis Correlates With Metastasis in Invasive Prostate Carcinoma," *American Journal of Pathology* 143, no. 2 (1993): 401–409.
40. M. K. Brawer, "Quantitative Microvessel Density: A Staging and Prognostic Marker for Human Prostatic Carcinoma," *Cancer* 78, no. 2 (1996): 345–349, [https://doi.org/10.1002/\(SICI\)1097-0142\(19960715\)78:2<345::AID-CNCR25>3.0.CO;2-V](https://doi.org/10.1002/(SICI)1097-0142(19960715)78:2<345::AID-CNCR25>3.0.CO;2-V).
41. M. Borre, B. Offersen, B. Nerstrøm, and J. Overgaard, "Microvessel Density Predicts Survival in Prostate Cancer Patients Subjected to Watchful Waiting," *British Journal of Cancer* 78, no. 7 (1998): 940–944, <https://doi.org/10.1038/bjc.1998.605>.
42. J. Sauvain, "Value of Power Doppler and 3D Vascular Sonography as a Method for Diagnosis and Staging of Prostate Cancer," *European Urology* 44, no. 1 (2003): 21–31, [https://doi.org/10.1016/S0302-2838\(03\)00204-5](https://doi.org/10.1016/S0302-2838(03)00204-5).
43. S. Zeng, S. Wu, C. Chen, et al., "Performance Characteristics of 3-D Power Doppler Ultrasound (3-D-PD) With the Virtual Organ Computer-Aided Analysis (VOCAL) Technique in the Detection of Prostate Cancer," *Ultrasound in Medicine & Biology* 48, no. 1 (2022): 91–97, <https://doi.org/10.1016/j.ultrasmedbio.2021.09.016>.
44. R. G. Barr, S. R. Wilson, A. Lyshchik, et al., "Contrast-Enhanced Ultrasound—State of the Art in North America: Society of Radiologists in Ultrasound White Paper," *Ultrasound quarterly* 36, no. 4S (2020): S1–S39, <https://doi.org/10.1097/RUQ.0000000000000515>.
45. D. B. Erlichman, A. Weiss, M. Koenigsberg, and M. W. Stein, "Contrast Enhanced Ultrasound: A Review of Radiology Applications," *Clinical Imaging* 60, no. 2 (2020): 209–215, <https://doi.org/10.1016/j.clinimag.2019.12.013>.
46. M. Seitz, C. Gratzke, B. Schlenker, et al., "Contrast-Enhanced Transrectal Ultrasound (CE-TRUS) With Cadence-Contrast Pulse Sequence (CPS) Technology for the Identification of Prostate Cancer," *Urologic Oncology: Seminars and Original Investigations* 29, no. 3 (2011): 295–301, <https://doi.org/10.1016/j.urolonc.2009.03.032>.
47. A. W. Postema, M. C. W. Gayet, R. J. G. van Sloun, et al., "Contrast-Enhanced Ultrasound With Dispersion Analysis for the Localization of Prostate Cancer: Correlation With Radical Prostatectomy Specimens," *World Journal of Urology* 38, no. 11 (2020): 2811–2818, <https://doi.org/10.1007/s00345-020-03103-4>.
48. M. P. J. Kuenen, M. Mischi, and H. Wijkstra, "Contrast-Ultrasound Diffusion Imaging for Localization of Prostate Cancer," *IEEE Transactions on Medical Imaging* 30, no. 8 (2011): 1493–1502, <https://doi.org/10.1109/TMI.2011.2125981>.
49. M. P. J. Kuenen, T. A. Saidov, H. Wijkstra, and M. Mischi, "Contrast-Ultrasound Dispersion Imaging for Prostate Cancer Localization by Improved Spatiotemporal Similarity Analysis," *Ultrasound in Medicine & Biology* 39, no. 9 (2013): 1631–1641, <https://doi.org/10.1016/j.ultrasmedbio.2013.03.004>.
50. M. Mischi, M. P. J. Kuenen, and H. Wijkstra, "Angiogenesis Imaging by Spatiotemporal Analysis of Ultrasound Contrast Agent Dispersion Kinetics," *IEEE Transactions on Ultrasonics, Ferroelectrics, and Frequency Control* 59, no. 4 (2012): 621–629, <https://doi.org/10.1109/TUFFC.2012.2241>.
51. R. R. Wildeboer, R. J. G. van Sloun, P. Huang, H. Wijkstra, and M. Mischi, "3-D Multi-Parametric Contrast-Enhanced Ultrasound for the Prediction of Prostate Cancer," *Ultrasound in Medicine & Biology* 45, no. 10 (2019): 2713–2724, <https://doi.org/10.1016/j.ultrasmedbio.2019.05.017>.
52. U. Hennrich and M. Eder, "68Ga]Ga-PSMA-11: The First FDA-Approved 68Ga-Radiopharmaceutical for PET Imaging of Prostate Cancer," *Pharmaceuticals* 14, no. 8 (2021): 713, <https://doi.org/10.3390/ph14080713>.
53. H. Song, A. Iagaru, and S. P. Rowe, "18F-DCFPyL PET Acquisition, Interpretation, and Reporting: Suggestions After Food and Drug Administration Approval," *Journal of Nuclear Medicine* 63, no. 6 (2022): 855–859, <https://doi.org/10.2967/jnumed.121.262989>.
54. R. H. Perera, A. de Leon, X. Wang, et al., "Real Time Ultrasound Molecular Imaging of Prostate Cancer With PSMA-Targeted Nanobubbles," *Nanomedicine: Nanotechnology, Biology and Medicine* 28 (2020): 102213, <https://doi.org/10.1016/j.nano.2020.102213>.
55. Y. Wang, A. C. De Leon, R. Perera, et al., "Molecular Imaging of Orthotopic Prostate Cancer With Nanobubble Ultrasound Contrast Agents Targeted to PSMA," *Scientific Reports* 11, no. 1 (2021): 4726, <https://doi.org/10.1038/s41598-021-84072-5>.
56. M. L. Oelze and J. Mamou, "Review of Quantitative Ultrasound: Envelope Statistics and Backscatter Coefficient Imaging and Contributions to Diagnostic Ultrasound," *IEEE Transactions on Ultrasonics, Ferroelectrics, and Frequency Control* 63, no. 2 (2016): 336–351, <https://doi.org/10.1109/TUFFC.2015.2513958>.
57. E. J. Feleppa, J. Mamou, C. R. Porter, and J. Machi, "Quantitative Ultrasound in Cancer Imaging," *Seminars in Oncology* 38, no. 1 (2011): 136–150, <https://doi.org/10.1053/j.seminoncol.2010.11.006>.
58. P. Gong, P. Song, C. Huang, J. Trzasko, and S. Chen, "System-Independent Ultrasound Attenuation Coefficient Estimation Using Spectra Normalization," *IEEE Transactions on Ultrasonics, Ferroelectrics, and Frequency Control* 66, no. 5 (2019): 867–875, <https://doi.org/10.1109/TUFFC.2019.2903010>.
59. F. Deeba, C. Schneider, S. Mohammed, et al., "A Multiparametric Volumetric Quantitative Ultrasound Imaging Technique for Soft Tissue Characterization," *Medical Image Analysis* 74 (2021): 102245, <https://doi.org/10.1016/j.media.2021.102245>.
60. M. F. Insana and T. J. Hall, "Parametric Ultrasound Imaging from Backscatter Coefficient Measurements: Image Formation and Interpretation," *Ultrasonic Imaging* 12, no. 4 (1990): 245–267, <https://doi.org/10.1177/016173469001200402>.
61. P. Muleki-Seya, A. Han, M. P. Andre, J. W. Erdman, and W. D. O'Brien, "Analysis of Two Quantitative Ultrasound Approaches," *Ultrasonic Imaging* 40, no. 2 (2018): 84–96, <https://doi.org/10.1177/0161734617729159>.
62. P. H. Tsui, C. K. Yeh, C. C. Chang, and Y. Y. Liao, "Classification of Breast Masses by Ultrasonic Nakagami Imaging: A Feasibility Study," *Physics in Medicine and Biology* 53, no. 21 (2008): 6027–6044, <https://doi.org/10.1088/0031-9155/53/21/009>.



63. P. H. Tsui, "Potential of Ultrasound Nakagami Imaging in Clinical Tissue Characterization," *Journal of Medical Ultrasound* 21, no. 21 (2013): 51–53, <https://doi.org/10.1016/j.jmu.2013.04.011>.
64. M. C. Ho, J. J. Lin, Y. C. Shu, et al., "Using Ultrasound Nakagami Imaging to Assess Liver Fibrosis in Rats," *Ultrasonics* 52, no. 2 (2012): 215–222, <https://doi.org/10.1016/j.ultras.2011.08.005>.
65. Z. Zhou, S. Wu, C. Y. Wang, H. Y. Ma, C. C. Lin, and P. H. Tsui, "Monitoring Radiofrequency Ablation Using Real-Time Ultrasound Nakagami Imaging Combined With Frequency and Temporal Compounding Techniques," *PLoS One* 10, no. 2 (2015): e0118030, <https://doi.org/10.1371/journal.pone.0118030>.
66. A. Sadeghi-Naini, E. Sofroni, N. Papanicolaou, et al., "Quantitative Ultrasound Spectroscopic Imaging for Characterization of Disease Extent in Prostate Cancer Patients," *Translational Oncology* 8, no. 1 (2015): 25–34, <https://doi.org/10.1016/j.tranon.2014.11.005>.
67. H. Tanoue, Y. Hagiwara, K. Kobayashi, and Y. Saijo, "Ultrasonic Tissue Characterization of Prostate Biopsy Tissues by Ultrasound Speed Microscope," in *2011 Annual International Conference of the IEEE Engineering in Medicine and Biology Society*, (2011), 8499–8502, <https://doi.org/10.1109/IEMBS.2011.6092097>.
68. H. Tanoue, Y. Hagiwara, K. Kobayashi, and Y. Saijo, "Echogenicity in Transrectal Ultrasound is Determined by Sound Speed of Prostate Tissue Components," in *2012 Annual International Conference of the IEEE Engineering in Medicine and Biology Society*, (2012) 460–463, <https://doi.org/10.1109/EMBC.2012.6345967>.
69. F. L. Lizzi, M. Greenebaum, E. J. Feleppa, M. Elbaum, and D. J. Coleman, "Theoretical Framework for Spectrum Analysis in Ultrasonic Tissue Characterization," *Journal of the Acoustical Society of America* 73, no. 4 (1983): 1366–1373, <https://doi.org/10.1121/1.389241>.
70. D. C. Morris, D. Y. Chan, T. H. Lye, et al., "Multiparametric Ultrasound for Targeting Prostate Cancer: Combining ARFI, SWEI, QUS and B-Mode," *Ultrasound in Medicine & Biology* 46, no. 12 (2020): 3426–3439, <https://doi.org/10.1016/j.ultrasmedbio.2020.08.022>.
71. D. Y. Chan, D. C. Morris, T. Lye, et al., "Evaluating Image Quality Improvement in Multiparametric Ultrasound Imaging of Prostate Cancer by Combining ARFI, SWEI, B-mode, and QUS," *2020 IEEE International Ultrasonics Symposium (IUS)* (2020): 1–4, <https://doi.org/10.1109/IUS46767.2020.9251796>.
72. M. Moradi, P. Mousavi, R. Siemens, E. Sauerbrei, A. Boag, and P. Abolmaesumi, "Prostate Cancer Probability Maps Based on Ultrasound RF Time Series and SVM Classifiers," in *Medical Image Computing and Computer-Assisted Intervention – MICCAI 2008. Lecture Notes in Computer Science*, eds. D. Metaxas, L. Axel, G. Fichtinger and G. Székely. Springer, 2008), 76–84, [https://doi.org/10.1007/978-3-540-85988-8\\_10](https://doi.org/10.1007/978-3-540-85988-8_10).
73. S. Azizi, S. Bayat, P. Yan, et al., "Deep Recurrent Neural Networks for Prostate Cancer Detection: Analysis of Temporal Enhanced Ultrasound," *IEEE Transactions on Medical Imaging* 37, no. 12 (2018): 2695–2703, <https://doi.org/10.1109/TMI.2018.2849959>.
74. S. J. Li, J. A. Barnes, P. Abolmaesumi, P. Mousavi, and H. P. Loock, "Micro-Vibrations Underlying Temporal Enhanced Ultrasound: The Effect of Scatterer Size and Elasticity," *Journal of Applied Physics* 125, no. 16 (2019): 164502, <https://doi.org/10.1063/1.5063666>.
75. F. Imani, P. Abolmaesumi, E. Gibson, et al., "Computer-Aided Prostate Cancer Detection Using Ultrasound RF Time Series: In Vivo Feasibility Study," *IEEE Transactions on Medical Imaging* 34, no. 11 (2015): 2248–2257, <https://doi.org/10.1109/TMI.2015.2427739>.
76. P. F. Fulgham, "Multiparametric Ultrasound-Targeted Biopsy Compares Favorably to Multiparametric MRI-Transrectal Ultrasound Fusion-Targeted Biopsy on Initial Biopsy of Men at Risk for Prostate Cancer," *World Journal of Urology* 36, no. 5 (2018): 713–718, <https://doi.org/10.1007/s00345-018-2187-9>.
77. C. K. Mannaerts, R. R. Wildeboer, S. Remmers, et al., "Multiparametric Ultrasound for Prostate Cancer Detection and Localization: Correlation of B-Mode, Shear Wave Elastography and Contrast Enhanced Ultrasound With Radical Prostatectomy Specimens," *Journal of Urology* 202, no. 6 (2019): 1166–1173, <https://doi.org/10.1097/JU.0000000000000415>.
78. D. C. Morris, D. Y. Chan, H. Chen, et al., "Multiparametric Ultrasound for the Targeting of Prostate Cancer using ARFI, SWEI, B-mode, and QUS," *2019 IEEE International Ultrasonics Symposium (IUS)* (2019): 880–883, <https://doi.org/10.1109/ULTSYM.2019.8926035>.
79. P. Pepe, L. Pepe, P. Panella, and M. Pennisi, "Can Multiparametric Ultrasound Improve Cognitive MRI/TRUS Fusion Prostate Biopsy," *Archivio italiano di urologia, andrologia: organo ufficiale [di] Societa italiana di ecografia urologica e nefrologica* 92, no. 2 (2020), <https://doi.org/10.4081/aiua.2020.2.89>.
80. R. R. Wildeboer, C. K. Mannaerts, R. J. G. van Sloun, et al., "Automated Multiparametric Localization of Prostate Cancer Based on B-Mode, Shear-Wave Elastography, and Contrast-Enhanced Ultrasound Radiomics," *European Radiology* 30, no. 2 (2020): 806–815, <https://doi.org/10.1007/s00330-019-06436-w>.
81. L. Liang, X. Zhi, Y. Sun, et al., "A Nomogram Based on a Multiparametric Ultrasound Radiomics Model for Discrimination Between Malignant and Benign Prostate Lesions," *Frontiers in Oncology* 11 (2021): 610785, <https://doi.org/10.3389/fonc.2021.610785>.
82. D. Y. Chan, D. C. Morris, T. Lye, et al., "Deep Neural Network for Multiparametric Ultrasound Imaging of Prostate Cancer," *2021 IEEE International Ultrasonics Symposium (IUS)* (2021): 1–4, <https://doi.org/10.1109/IUS52206.2021.9593332>.
83. N. Jung, R. G. DiNatale, J. Frankel, et al., "The Role of Multiparametric Ultrasound in the Detection of Clinically Significant Prostate Cancer," *World Journal of Urology* 41 (2022): 663–671, <https://doi.org/10.1007/s00345-022-04122-z>.
84. D. Y. Chan, D. C. Morris, S. R. Moavenzadeh, et al., "Multiparametric Ultrasound Imaging of Prostate Cancer Using Deep Neural Networks," *Ultrasound in Medicine & Biology* 50, no. 11 (2024): 1716–1723, <https://doi.org/10.1016/j.ultrasmedbio.2024.07.012>.
85. P. Chen, S. Turco, Y. Wang, et al., "Can 3D Multiparametric Ultrasound Imaging Predict Prostate Biopsy Outcome?," *Ultrasound in Medicine and Biology (Oxford)* 50, no. 8 (2024): 1194–1202, <https://doi.org/10.1016/j.ultrasmedbio.2024.04.007>.
86. D. Eldred-Evans, P. Burak, M. J. Connor, et al., "Population-Based Prostate Cancer Screening With Magnetic Resonance Imaging or Ultrasonography: The IP1-PROSTAGRAM Study," *JAMA Oncology* 7, no. 3 (2021): 395–402, <https://doi.org/10.1001/jamaoncol.2020.7456>.
87. A. Grey and H. U. Ahmed, "Multiparametric Ultrasound in the Diagnosis of Prostate Cancer," *Current Opinion in Urology* 26, no. 1 (2016): 114–119, <https://doi.org/10.1097/MOU.0000000000000245>.
88. A. D. R. Grey, R. Scott, B. Shah, et al., "Multiparametric Ultrasound Versus Multiparametric MRI to Diagnose Prostate Cancer (CADMUS): A Prospective, Multicentre, Paired-Cohort, Confirmatory Study," *Lancet Oncology* 23, no. 3 (2022): 428–438, [https://doi.org/10.1016/S1470-2045\(22\)00016-X](https://doi.org/10.1016/S1470-2045(22)00016-X).
89. M. Moradi, S. E. Salcudean, S. D. Chang, et al., "Multiparametric MRI Maps for Detection and Grading of Dominant Prostate Tumors," *Journal of Magnetic Resonance Imaging* 35, no. 6 (2012): 1403–1413, <https://doi.org/10.1002/jmri.23540>.
90. C. M. Laurence Klotz, "Can High Resolution Micro-Ultrasound Replace MRI in the Diagnosis of Prostate Cancer?," *European Urology Focus* 6, no. 2 (2020): 419–423, <https://doi.org/10.1016/j.euf.2019.11.006>.
91. L. Klotz, G. Lughezzani, D. Maffei, et al., "Comparison of Micro-Ultrasound and Multiparametric Magnetic Resonance Imaging for Prostate Cancer: A Multicenter, Prospective Analysis," *Canadian Urological Association journal = Journal de l'Association des urologues du Canada* 15, no. 1 (2021): 11, <https://doi.org/10.5489/cuaj.6712>.

92. P. Sountoulides, N. Pyrgidis, S. A. Polyzos, et al., "Micro-Ultrasound-Guided vs Multiparametric Magnetic Resonance Imaging-Targeted Biopsy in the Detection of Prostate Cancer: A Systematic Review and Meta-Analysis," *Journal of Urology* 205, no. 5 (2021): 1254–1262, <https://doi.org/10.1097/JU.0000000000001639>.
93. C. You, X. Li, Y. Du, et al., "The Microultrasound-Guided Prostate Biopsy in Detection of Prostate Cancer: A Systematic Review and Meta-Analysis," *Journal of Endourology* 36, no. 3 (2022), <https://doi.org/10.1089/end.2021.03>.
94. J. Pensa, W. Brisbane, A. Kinnaird, et al., "Evaluation of Prostate Cancer Detection Using Micro-Ultrasound Versus MRI Through Co-Registration to Whole-Mount Pathology," *Scientific Reports* 14, no. 1 (2024): 18910, <https://doi.org/10.1038/s41598-024-69804-7>.
95. L. Klotz, G. Andriole, H. Cash, et al., "Optimization of Prostate Biopsy - Micro-Ultrasound Versus MRI (OPTIMUM): A 3-Arm Randomized Controlled Trial Evaluating the Role of 29 MHz Micro-Ultrasound in Guiding Prostate Biopsy in Men With Clinical Suspicion of Prostate Cancer," *Contemporary Clinical Trials* 112 (2022): 106618, <https://doi.org/10.1016/j.cct.2021.106618>.
96. D. Rohrbach, B. Wodlinger, J. Wen, J. Mamou, and E. Feleppa, "High-Frequency Quantitative Ultrasound for Imaging Prostate Cancer Using a Novel Micro-Ultrasound Scanner," *Ultrasound in Medicine & Biology* 44, no. 7 (2018): 1341–1354, <https://doi.org/10.1016/j.ultrasmedbio.2018.02.014>.
97. T. A. Aleef, R. Vassallo, Q. Zeng, et al., "Implementation of Shear Wave and Strain Elastography With Micro-Ultrasound," *2023 IEEE International Ultrasonics Symposium (IUS)* (2023): 1–6, <https://doi.org/10.1109/IUS51837.2023.10306532>.
98. R. Vassallo, T. A. Aleef, V. Desaioudar, et al., "Simplifying Prostate Elastography Using Micro-ultrasound and Transfer Function Imaging," in *Simplifying Medical Ultrasound*, eds. A. Gomez, B. Khanal, A. King, A. Namburete. Springer Nature Switzerland, (2025), 14–23, [https://doi.org/10.1007/978-3-031-73647-6\\_2](https://doi.org/10.1007/978-3-031-73647-6_2).
99. S. Schaer, A. Rakauskas, J. Dagher, et al., "Assessing Cancer Risk in the Anterior Part of the Prostate Using Micro-Ultrasound: Validation of a Novel Distinct Protocol," *World Journal of Urology* 41, no. 11 (2023): 3325–3331, <https://doi.org/10.1007/s00345-023-04591-w>.
100. G. Eure, D. Fanney, J. Lin, B. Wodlinger, and S. Ghai, "Comparison of Conventional Transrectal Ultrasound, Magnetic Resonance Imaging, and Micro-Ultrasound for Visualizing Prostate Cancer in an Active Surveillance Population: A Feasibility Study," *Canadian Urological Association journal = Journal de l'Association des urologues du Canada* 13, no. 3 (2019): 70, <https://doi.org/10.5489/cuaj.5361>.
101. X. Yang and L. Xiang, "Photoacoustic Imaging of Prostate Cancer," *Journal of Innovative Optical Health Sciences* 10, no. 04 (2017): 1730008, <https://doi.org/10.1142/S1793545817300087>.
102. S. H. El-Gohary, M. K. Metwally, S. Eom, S. H. Jeon, K. M. Byun, and T. S. Kim, "Design Study on Photoacoustic Probe to Detect Prostate Cancer Using 3D Monte Carlo Simulation and Finite Element Method," *Biomedical Engineering Letters* 4, no. 3 (2014): 250–257, <https://doi.org/10.1007/s13534-014-0150-2>.
103. C. H. Lee, O. Akin-Olugbade, and A. Kirschenbaum, "Overview of Prostate Anatomy, Histology, and Pathology," *Endocrinology and Metabolism Clinics of North America* 40, no. 3 (2011): 565–575, <https://doi.org/10.1016/j.ecl.2011.05.012>.
104. D. J. Faber, E. G. Mik, M. C. G. Aalders, and T. G. van Leeuwen, "Light Absorption of (oxy-)Hemoglobin Assessed by Spectroscopic Optical Coherence Tomography," *Optics Letters* 28, no. 16 (2003): 1436–1438, <https://doi.org/10.1364/OL.28.001436>.
105. V. S. Dogra, B. K. Chinni, K. S. Valluru, et al., "Multispectral Photoacoustic Imaging of Prostate Cancer: Preliminary Ex-Vivo Results," *Journal of Clinical Imaging Science* 3 (2013): 41, <https://doi.org/10.4103/2156-7514.119139>.
106. J. Levi, A. Sathirachinda, and S. S. Gambhir, "A High-Affinity, High-Stability Photoacoustic Agent for Imaging Gastrin-Releasing Peptide Receptor in Prostate Cancer," *Clinical Cancer Research* 20, no. 14 (2014): 3721–3729, <https://doi.org/10.1158/1078-0432.CCR-13-3405>.
107. V. Dogra, B. Chinni, S. Singh, et al., "Photoacoustic Imaging With an Acoustic Lens Detects Prostate Cancer Cells Labeled With PSMA-Targeting Near-Infrared Dye-Conjugates," *Journal of Biomedical Optics* 21, no. 6 (2016): 066019, <https://doi.org/10.1117/1.JBO.21.6.066019>.
108. A. Agarwal, S. W. Huang, M. O'Donnell, et al., "Targeted Gold Nanorod Contrast Agent for Prostate Cancer Detection by Photoacoustic Imaging," *Journal of Applied Physics* 102, no. 6 (2007): 064701, <https://doi.org/10.1063/1.2777127>.
109. G. Xu, M. Qin, A. Mukundan, et al., "Prostate Cancer Characterization by Optical Contrast Enhanced Photoacoustics," *Proceedings of SPIE - The International Society for Optical Engineering* (2016): 127–132, <https://doi.org/10.1117/12.2213064>.
110. R. Markwalder and J. C. Reubi, "Gastrin-Releasing Peptide Receptors in the Human Prostate: Relation to Neoplastic Transformation," *Cancer Research* 59, no. 5 (1999): 1152–1159.
111. A. Ghosh and W. D. W. Heston, "Tumor Target Prostate Specific Membrane Antigen (PSMA) and Its Regulation in Prostate Cancer," *Journal of Cellular Biochemistry* 91, no. 3 (2004): 528–539, <https://doi.org/10.1002/jcb.10661>.
112. S. R. Kothapalli, G. A. Sonn, J. W. Choe, et al., "Simultaneous Transrectal Ultrasound and Photoacoustic Human Prostate Imaging," *Science Translational Medicine* 11, no. 507 (2019): eaav2169, <https://doi.org/10.1126/scitranslmed.aav2169>.
113. A. Raabe, J. Beck, R. Gerlach, M. Zimmermann, and V. Seifert, "Near-Infrared Indocyanine Green Video Angiography: A New Method for Intraoperative Assessment of Vascular Flow," *Neurosurgery* 52, no. 1 (2003): 132–139, <https://doi.org/10.1097/00006123-200301000-00017>.
114. S. L. Owens, "Indocyanine Green Angiography," *British Journal of Ophthalmology* 80, no. 3 (1996): 263–266.